Journal of Saudi Chemical Society (2015) 19, 217–226

King Saud University

Journal of Saudi Chemical Society

www.ksu.edu.sa
www.sciencedirect.com

ORIGINAL ARTICLE

Syntheses, structural elucidation, thermal properties, theoretical quantum chemical studies (DFT) and biological studies of barbituric–hydrazone complexes

Amina A. Soayed [a,*,1], **Heba M. Refaat** [a], **Leena Sinha** [b]

[a] *Faculty of Science, Alexandria University, Chemistry Department, P.O. Box 426-Ibrahimia, Alexandria 21321, Egypt*
[b] *Department of Physics, University of Lucknow, Lucknow, India*

Received 9 April 2014; revised 13 May 2014; accepted 13 May 2014
Available online 24 May 2014

KEYWORDS

ESR;
TGA–DTA;
Biological activity;
Quantum chemical calculations

Abstract Condensation of barbituric acid with hydrazine hydrate yielded barbiturichydrazone (L) which was characterized using IR, ^{1}H NMR and mass spectra. The Co(II), Ni(II) and Cu(II) complexes derived from this ligand have been synthesized and structurally characterized by elemental analyses, spectroscopic methods (IR, UV–Vis and ESR) and thermal analyses (TGA, DTG and DTA) and the structures were further elucidated using quantum chemical density functional theory. Complexes of L were found to have the ML.nH$_2$O stoichiometry with either tetrahedral or octahedral geometry. The ESR data showed the Cu(II) complex to be in a tetragonal geometry. Theoretical investigation of the electronic structure of metal complexes at the TD-DFT/B3LYP level of theory has been carried out and discussed. The fundamental vibrational wavenumbers were calculated and a good agreement between observed and scaled calculated wavenumbers was achieved. Thermal studies were performed to deduce the stabilities of the ligand and complexes. Thermodynamic parameters, such as the order of reactions (n), activation energy ΔE^*, enthalpy of reaction ΔH^* and entropy ΔS^* were calculated from DTA curves using Horowitz–Metzger method. The ligand L and its complexes have been screened for their antifungal and antibacterial activities and were found to possess better biological activities compared to those of unsubstituted barbituric acid complexes.

* Corresponding author. Tel.: +20 1005297350; fax: +20 3 39 11 794.
E-mail address: amsoayed@yahoo.com (A.A. Soayed).
[1] Present address: University of Dammam, Chemistry Department, Saudi Arabia. Tel.: +966 545996300.

Peer review under responsibility of King Saud University.

Production and hosting by Elsevier

1. Introduction

Considerable attention has been directed to artificial receptors for biologically active molecules [1]. From the most suitable compounds for this purpose are the derivatives of barbituric acid which are members of the pyrimidine family. However, their biological activity is mainly attributed to tautomeric,

http://dx.doi.org/10.1016/j.jscs.2014.05.003

acid-base equilibrium and to the nature of the substituents [1]. Moreover, compounds containing pyrimidine ring play an important role in many biological systems, where they exist in nucleic acids, several vitamins, coenzymes and antibiotics [2]. Nucleic acids are related to antimetabolites used in anti-carcinogenic chemotherapy [3]. Some novel pyrimidine-2,4-diones were found to have good anti-fungal activity and are thus potential agents to treat infections [4]. Metal complexes of pyrimidines as well have a great variety of biological activities such as antimalarial, antibacterial, antitumor and antiviral activities [5–8].

Well known pyrimidines are barbituric acid derivatives that constitute a class of drugs that have diverse applications such as sedatives, hypnotics and anticonvulsants and are also employed for anesthesia [9,10]. They are also used for the treatment of anxiety, epilepsy and other psychiatric disorders and possess effects on the motor and sensory functions [11,12]. Barbituric acid derivatives also exert important action on the central nervous system (CNS) [13] and have found totally new biomedicinal applications in fields such as cancer and AIDS therapy [14]. Their activity might be influenced by complex formation. Some of barbituric acid derivatives as well were found to reduce body weight, liver weight, visceral fat and regulated serum levels of biochemical markers [15].

Moreover, hydrazones and their derivatives have interesting biological properties, such as anti-inflammatory, analgesic, anticonvulsant, antituberculous, antitumor, anti-HIV and antimicrobial activities [16]. Hydrazones containing amide groups such as isatin act as inhibitors and cause an arrest of the cell cycle and exhibit a selective killing effect on several tumor cell lines [17].

Because of the wide range of medicinal applications of barbiturates and hydrazones and their ability to coordinate with transition metal ions, syntheses of their metal complexes and the study of such complexes may lead to a greater understanding of the role of these compounds in biological systems, and may also contribute to the development of new metal-based chemotherapeutic agents. In this manuscript, we report on synthesis and solid state structure of the chelation of first row transition metal ions with barbituric containing hydrazone ligand as this field to the best of our knowledge has not been exploited before.

2. Experimental

2.1. Materials and reagents

All chemicals used were of analytical reagent grade (AR). ^{1}H NMR spectrum was recorded on a Varian EM 390 90 NMR spectrometer (Micro Analysis Center, Cairo University, Egypt) using DMSO-d^6 (Merck) as a solvent and tetramethylsilane (TMS) as an internal standard at room temperature. Mass spectral measurement of the synthesized compound was done on a DI Analysis Shimadzu Qp-2010 Plus (Micro Analysis Center, Cairo University, Egypt). Spectrophotometric measurements were carried out using an automated spectrophotometer UV/VIS Perkin-Elmer Model Lambda 20, and ranged from 200 to 1200 nm. Elemental microanalyses of the separated solid chelates for C, H and N were performed by the Micro analytical Center, Cairo University using the usual methods of analyses. The metal ion content was determined using both volumetric analyses by atomic absorption method using spectrophotometer 850-Fisher Jarrell ash computer controlled. Infrared spectra were recorded on a Perkin-Elmer FT-IR type 1650 spectrophotometer in wavenumber region 4000–200 cm^{-1}. The spectra were recorded as KBr pellets. The thermogravimetric analyses (TGA, DTG and DTA) were carried out in a dynamic nitrogen atmosphere (20 mL min^{-1}), with a heating rate of 10 °C min^{-1} using LINSELS STA PT 1000 thermal analyzer. The ESR (X-band) spectrum for the poly-crystalline sample was recorded at room temperature using a Varian E-12 spectrometer and DPPH as an external standard.

2.2. Procedures

2.2.1. Synthesis of ligand: (L)

A hot solution (70 °C) of barbituric acid (1.12 g, 10 mmol) dissolved in the least amount of water was mixed with a hot solution (70 °C) of hydrazine hydrate (0.32 g, 10 mmol) in 50 mL of ethanol to which (0.40 g, 10 mmol) of NaOH was added. The resulting mixtures were left under reflux with stirring for at least 7–8 h after which the red solid product (L) was formed, filtered, washed with diethyl ether, and then dried in vacuum over anhydrous calcium chloride.

2.2.2. Syntheses of metal complexes

The metal complexes of (L) were prepared by the addition of a hot solution (70 °C) of the appropriate metal chloride (10 mmol); ($CoCl_2{\cdot}6H_2O$, 2.37 g, $NiCl_2{\cdot}6H_2O$, 2.37 g, $CuCl_2.2H_2O$, 1.70 g) in ethanol (25 ml) to a hot solution (70 °C) of the ligand (10 mmol) in the same solvent (25 ml). The medium was controlled by adding NH_3 solution till pH is between 9 and 10 to prepare weak alkaline medium. The resulting mixtures were stirred under reflux for 2–3 h whereupon the complexes precipitated, were collected by filtration, washed with a 1:1 ethanol–water mixture followed by diethyl ether and then dried in vacuum over anhydrous calcium chloride.

The analytical data for L complexes were as follows: $[CoL.H_2O]_2$, (% Calcd. found): [(Co: 27.09; 26.98); (C: 22.15; 22.20); (N: 25.84; 25.47); H: 2.76; 3.07)]; λ_{max} (nm) = 432, 579, 638. For $[NiL.3H_2O]$ H_2O, (% Calcd. found): [(Ni: 21.58; 21.49); (C: 17.58; 17.37); (N: 20.52; 20.39); (H: 4.39; 4.17)]; λ_{max} (nm) = 433, 460, 495. For $[CuL.H_2O]_2$, (% Calcd. found): [(Cu: 28.68; 28.36); (C: 21.66; 21.60); N: 25.28; 24.94); (H: 2.71; 2.93)];. λ_{max} (nm) = 484, 684, 979.

2.3. Biological activity

Antimicrobial activities of the tested complexes were determined using a modified Kirby–Bauer disk diffusion method [18]. 100 µl of the test bacteria or fungi were grown in 10 ml of fresh media until they reached a count of approximately 108 cells/ml for bacteria or 105 cells/mL for fungi [19]. 100 µl of microbial suspension was spread into agar plates corresponding to the two in which they were maintained. Plates incubated with filamentous fungi as *Aspergillus flavus* at 25 °C for 48 h; Gram (+) bacteria as *Staphylococcus Aureus*, Gram (−) bacteria as *Escherica coli* were incubated at 35–37 °C for 24–48 h and yeast as *Candida albicans* incubated at 30 °C for 24–48 h and then the diameters of the inhibition zones were measured in millimeters [18].

2.4. Quantum chemical calculations

Since single crystal X-ray structure for the ligand and its complexes was not available, so, quantum chemical calculations were utilized to find the geometrically optimized structures of these complexes. Optimization of geometries was done with the density functional theory method (DFT) using the GAUSSIAN 09 program package [20], as DFT methods are very effective in modeling compounds and have good experimental correlations with the IR frequencies. The DFT method was treated according to hybrid Becke's three parameter and the Lee–Yang–Parr function (B3LYP), the most popular density functional method [21–23], using the 6–31G (d) basis set for the H, C, N and O atoms and LANL2DZ basis set for the metal centers in the gas phase. The vibrational assignments of the normal modes were made by combining the results of the Gaussview 5 molecular visualization program with the VEDA 4 program [24,25]. Theoretical investigation of the electronic structure of metal complexes has also been carried out, the frontier orbital has been plotted and discussed using time-dependent DFT.

3. Results and discussion

3.1. Characterization of ligand and metal(II) complexes

Some authors discussed the formation of hydrazones by the direct reaction between hydrazines and barbituric acid where a series of hydrazones bearing an amide group were prepared by Belskaya et al. [26]. Vvedenskii et al. [27] have shown that the condensation of barbituric acid with hydrazines affords barbituric acid 2-hydrazones due to the ketonic character of the 2-carbonyl group. On the other hand, Lehn et al. [28] have also shown that condensation of cyclic ketones with hydrazines yields the corresponding hydrazones or its hydrazino-enone tautomer. The prepared hydrazones of barbituric acid retain their acidic properties.

In this manuscript, condensation of barbituric acid with hydrazine hydrate yielded the ligand – L. The structure of the ligand L was elucidated using IR, NMR and mass spectra, together with the use of theoretical quantum chemical DFT method.

3.1.1. Geometry

Barbituric–hydrazone ligand (L) can either exist in the keto or enol form, Fig. 1, but theoretically the keto form (Ground state energy −525.49430 a.u.) was found to be more stable than the enol form (Ground state energy −525.44869 a.u.). This indicates that the ligand is present predominately in the keto form. However, theoretical calculations have shown that chelation took place through the enol form of the ligand and metal ions, Table 1. The ML.nH_2O complexes were formed by the binding of the metal ions to the –NH_2 group of the hydrazone and the oxygen atom of the barbiturate moiety where a five membered ring was formed. Geometry optimization is one of the most important steps in the quantum chemical calculations. The structure of the ligand as well as the complexes were fully optimized using density functional theory. The accuracy of the geometry optimization was verified by wave-number calculations. Positive values of all the calculated vibrational wave numbers confirmed the geometries to be located on true local minima on the potential energy surface. Positive wavenumbers established the stability of the structures at minimum energy. The selected optimized bond length and bond angles for Cu(II), Co(II) and Ni(II) metal complexes are gathered in Table 1.

The calculated N—N bond length in the ligand (1.375 Å) was found to be shorter than the usual hydrazine N—N bond length (1.38 Å), but is closer to other similar molecules containing the N—N moiety, such as dihydrazones [29].

On the other hand, it is documented that the formation of 3-fold/or 2-fold hydrogen bonds by the C—O groups results in the elongation of this bond from the predicted carbon–oxygen bond length (1.26 Å) up to 1.320 Å [30]. The C1—O1 and C2—O2 bond lengths determined from DFT calculations in "L" seems to have (1.335 and 1.345 Å) values indicating the contribution of C—O groups of barbituric acid moiety in H-bonds [31,32].

The C2—N2 and C3—N3 bond lengths were found to be 1.285 and 1.287 Å, which are comparable with those found in the literature (1.20–1.23 Å).

The N1–C2–N2 angle in the ligand had increased to a value of 128.2°, whereas C2–N2–C3 and N2–C3–C4 angle had decreased to 116.8° and 118.5°, respectively, due to the presence of H-bonding between O2 and a neighboring hydrogen from another ligand molecule, whereas, the C3–C4–C1 angle had nearly the usual bond angle of tetrahedral bonds (108.8°). Upon complexation, the bond length C2—N2 showed elongation as compared to the ligand, which may be due to its relative binding to the metal ions. The dihedral angle C2–N2–C3–N3 was also found to increase giving more planarity to the

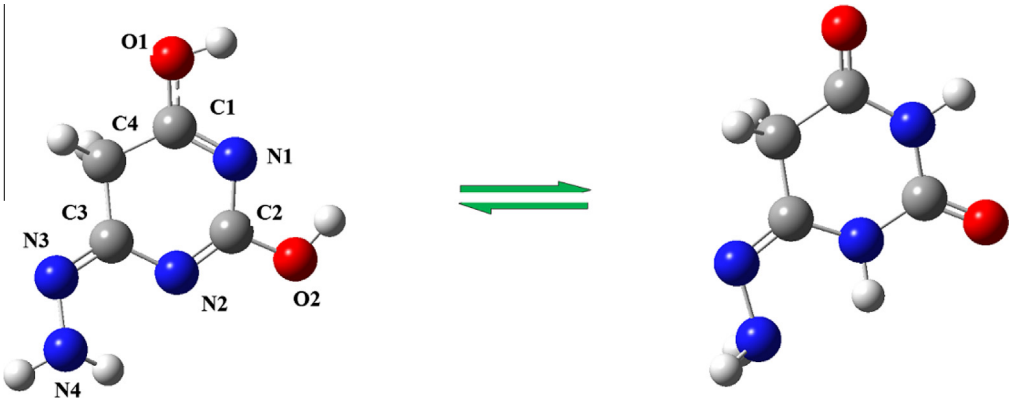

Figure 1 Ketoenol forms of the ligand.

Table 1 Selected Optimized bond lengths (Å), bond angles and dihedral angles (°) of the studied systems obtained at the B3LYP/6-31G(d)/LANL2DZ level.

Parameter	Ligand	Cu(II) complex	Co (II) complex	Ni(II) complex
Bond lengths (Å)				
N1–C2	1.405	1.402	1.420	1.409
C2–N2	1.285	1.365	1.338	1.355
N2–C3	1.396	1.363	1.370	1.398
C3–N3	1.287	1.330	1.314	1.286
N3–N4	1.375	1.310	1.345	1.384
C3–C4	1.516	1.500	1.505	1.503
C1–O1	1.335	1.336	1.339	1.348
C2–O2	1.345	1.253	1.276	1.257
A*ν*(M–N) (M═Cu, Co, Ni)	–	2.007	1.868	1.865
Bond angles				
N1–C2–N2	128.2	121.1	120.2	120.5
C2–N2–C3	116.8	121.2	122.2	121.5
N2–C3–N3	122.8	119.4	117.5	119.2
N2–C3–C4	118.5	120.6	120.1	118.1
C3–C4–C1	108.8	109.5	109.1	109.2
Dihedral angle				
C2–N2–C3–N3	162.3	176.8	178.4	171.9

five membered ring formed on complexation. As the X-ray structure of the ligand and its complexes was not available, the optimized parameters have been compared with other similar molecules [33,34].

3.1.2. IR (Experimental and Theoretical calculations), ^1H NMR and mass spectra

Theoretical calculations of the IR spectra of the ligand "L" and its metal complexes were carried out, Table 2. The calculated IR spectral intensities were used to convolute all the predicted vibrational modes using a pure Lorentzian line shape with a FWHM bandwidth of 10 cm^{-1}, to conjure up the spectra. Vibrational assignments of selected modes, compared with the experimental spectra, are given in Figs. 2–4, Table 2. The vibrational wavenumber assignments have been carried out by combining the results of the Gaussview 5 program [24] and the VEDA 4 program [25]. The calculated harmonic wavenumbers are usually higher than the corresponding experimental quantities. This observed dissimilarity between theory and experiment could be a consequence of the anharmonicity and of the general tendency of the quantum chemical methods to overestimate the force constants at the exact equilibrium geometry. These discrepancies are taken care of either by computing anharmonic corrections explicitly or by introducing scalar field, or even by direct scaling of the calculated wavenumbers with a proper scaling factor [35,36]. The wavenumbers from the B3LYP calculations have been scaled by a factor of 0.96, which is a typical correction factor for B3LYP frequencies [37].

The experimental IR spectrum of the ligand showed frequencies in the range 3691–3151 cm^{-1} corresponding to *ν*(O—H) as well as *ν*NH_2 stretching vibrations. The broad shape of this band confirmed the formation of a hydrogen bond. The discrepancy between the theoretical and experimental wavenumber of O–H group vibration in both the ligand and its complexes was ascribed to the formation of intermolecular H-bonding. Theoretical calculations also showed that the ligand may exist in tautomeric forms and associated structures through inter- and intramolecular hydrogen bonds. Bands around 3350–3750 cm^{-1} in metal complexes are attributed to the presence of coordinated water molecules through intra- or intermolecular H-bonding [38]. The spectral positions of asymmetric and symmetric C—H stretching vibrations of the methylene group were found to be comparable (2987 and 2885^{-1}) with those of aromatic C–H ring stretching vibrations (2900–3000 and 2800–2900 cm^{-1}) [39,40]. The *ν*(C═O) and *ν*(N—H) stretching bands of barbituric acid disappeared in the studied hydrazone ligand (L), indicating its transformation to the enol form.

The bands due to *ν*C1═N, *ν*C2═N of barbituric acid moiety are observed in the range 1592–1699 cm^{-1} in the ligand and its complexes [41]. New bands at frequencies 400–450 and 610–675 cm^{-1} in the spectra of the complexes were obtained, which were tentatively assigned to *ν*M–N and, *ν*M–O vibrations [42], respectively.

^1H NMR spectroscopy is used for structure and functional determination of molecules. One of the most common solvents used in NMR is dimethylsulfoxide (DMSO), which is a polar solvent. The oxygen atoms in DMSO are often involved in strong hydrogen bonding interactions with acidic protons of solute molecules (usually protons of –OH or –NH moieties), as those found in barbituric acid. DMSO withdraws the electron density from the hydrogen atoms present and so, these protons signals are shifted downfield [43,44].

^1H NMR spectrum of –L, was consistent with its deduced structure. The signals of the 2NH protons (N–1 and N–2) of the pyrimidine ring were observed at *δ* 10.69 and 10.28 ppm [45]. These chemical shifts were observed to be at a downfield shifting than expected (6.41–6.61 ppm) due to the intermolecular interactions of barbituric moiety with DMSO [46,47]. Hydrogen bonded –OH appears at *δ* 7.76–8.00 ppm and the enolic proton of the pyrimidine ring resonated in the range *δ* 8.5–9.1 ppm [46].

A broad weak signal at *δ* 4.79 ppm is due to the NH_2 protons of the hydrazone group and that at *δ* 5.18 ppm is due to

Table 2 Selected IR bands of the ligand and its complexes.

Mode	Ligand		Cu(II) complex			Co (II) Complex			Ni(II) complex	
	Expt.	Calc.	Expt.	Calc.		Expt.	Calc.		Expt.	Calc.
ν(O1–H)	3691	3579	3428	3593	3506	3672	3595	3531	3672	3594
ν(N4–H)	3316	3464	3350	3311	3289	3294	3367	3365	3294	3305
	3151									
ν_{as}(C4–H)	2987	3012	3180	2978	2948	2972	2971	2934	2987	2964
ν_{s}(C4–H)	2885	2877	2700	2882	2840	2901	2866	2842	2901	2878
ν(C1═N1)	1693	1671	1592	1656	1637	1674	1651	1622	1699	1671
						1614				
ν(C2═N2)	1658									
ν(C2–O2)		1358	1517	1560	1495	1569-	1519		1565	1557
ν(C3═N3)	1593	1635	–	1400	1376	1452	1494	1475	1615	1624
(N3–N4–H)	1347	1311	1434	1428	1376	1390	1370	1366	1342	1319
sc CH_2	1441	1425	–	1421	1411	1348	1431	1430	–	1421
Twist CH_2	1130	1148	–	1135	1132	1282	1152	1145	–	1145
Rock CH_2	1214	1256	1351	1328	1240	1224	1261	1250	1283	1269
ν(N3═N4)	1106	1100	1257	1267	1186	1182	1152	1123	1056	1045
Ring trigonal bending	809	885	–	894	889	866	948	945	–	950
	969									
(C3–N3–N4)	678	685	779	728	708	770	745	609	726	748
Wag (O1–H)	653	655	664	664	444	680	481	401	–	440
			616			654				

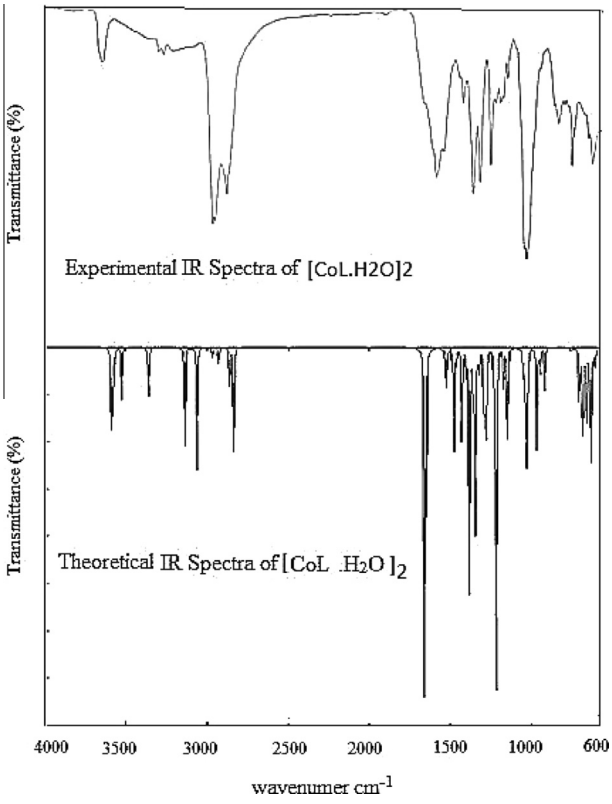

Figure 2 Experimental and theoretical IR spectra of $[CoL.H_2O]_2$.

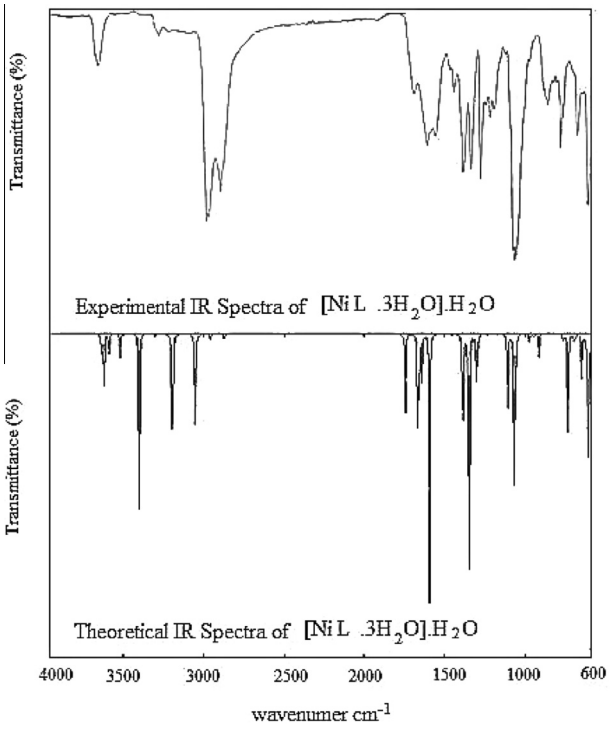

Figure 3 Experimental and theoretical IR spectra of $[NiL.3H_2O]H_2O$.

hydrogens of pyrimidine ring, respectively [48]. Due to the low solubility of L, weak signals in its ^{1}H NMR spectrum were obtained, whereas ^{13}C NMR could not be traced.

Mass spectra are another tool that provides a vital clue for elucidating the structure of compounds. The mass spectrum of L showed relatively small or moderate molecular ion peaks. The spectrum showed the molecular ion peak at m/z = 142. The base peak at m/z = 64 is due to $(NCN^{+} + 2C^{+})$ or $(C.C(N).NC)^{+}$ ions. Other intense peaks were at m/z = 55, 57, 69 and 128, respectively. The different fragmentation pathways of the ligand give peaks at different other mass numbers at 80, 85, 95, 97, 111 and 119. The intensity of these peaks reflects the stability and abundance of the ions [49].

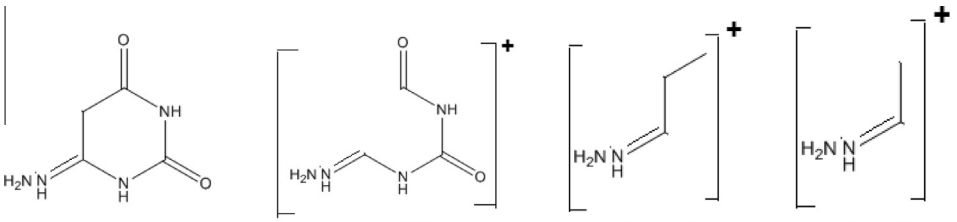

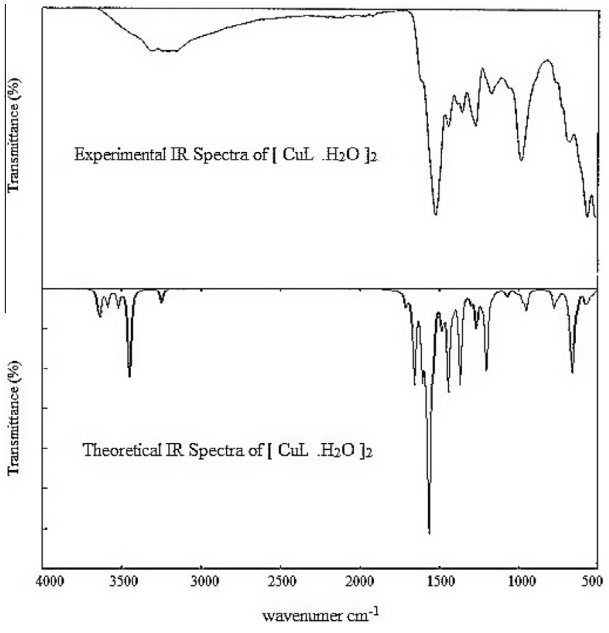

Figure 4 Experimental and theoretical IR spectra of $[CuL.H_2O]_2$.

3.1.3. Electronic properties and electronic absorption spectra

The Frontier orbitals, highest occupied molecular orbital (HOMO) and lowest unoccupied molecular orbital (LUMO) are important factors in quantum chemistry as these determine the way the molecule interacts with other species. The HOMO and LUMO are known as the electron donor and electron acceptor. The frontier orbital gap is used as an indicator for chemical reactivity and kinetic stability of the molecule. A molecule with a small frontier orbital gap is more polarizable and is generally associated with a high chemical reactivity, low kinetic stability, and is also termed as soft molecule [50]. In order to get a further understanding of the structures of ligand (L) and its complexes, their electronic structures have been probed. The energy of the HOMO and LUMO orbitals and their orbital energy gap are calculated using the TD-DFT method, and the pictorial illustrations of these frontier orbitals for the ligand and the complexes are shown in Fig. 5. The orbital wave functions switch from positive to negative whenever they go through a node. Positive and negative regions are shown by green and red colors respectively. The energy gap in the case of $[CuL.H_2O]_2$ is found to be least (0.92546 eV) while $[NiL.3H_2O].H_2O$ has the maximum value at 3.47380 eV, which implies $[CuL.H_2O]_2$ has a higher chemical activity than the other complexes.

The electronic spectral measurements were performed to assign the stereo chemistries of metal ions in the complexes based on the positions and number of d–d transition peaks. λ_{max} of the metal complexes of Co(II), Ni(II) and Cu(II) were recorded at room temperature as Nujol mull. For the $[CoL.H_2O]_2$ complex, λ_{max} were observed at 432, 579 and 638 nm assignable to $^4A_2 \rightarrow {}^4T_1$ (P), $^4A_2 \rightarrow {}^4T_1$ (F) and $^4A_2 \rightarrow {}^4T_2$ transitions, respectively, which are in conformity with tetrahedral arrangement around Co(II) ion [51].

$[NiL.3H_2O]$ H_2O gave three bands at λ_{max} 460, 495 and 1000 nm assigned to $^3A_{2g} \rightarrow {}^3T_{1g}$ (P), $^3A_2g \rightarrow {}^3T_{1g}$ (F) and $^3A_{2g} \rightarrow {}^3T_{2g}$ favoring the octahedral geometry [42,52,53]. On the other hand, $[CuL.H_2O]_2$ showed λ_{max} at 484, 684 and 979 nm which is in conformity with tetrahedral geometry [54].

3.1.4. ESR spectra

The X-band ESR spectrum of the Cu(II) complex was studied in the 2300–4000G region, in polycrystalline form, Fig. 6. The spectrum of the $[CuL.H_2O]_2$ complex exhibited signals attributed to axial spectra with ($g_{||}$ = 2.253 and 2.243) assigning a d_{xy} ground state with a G value amounting to 2.09. The G-value is less than 4, ($G = g_{||} - 2/g_{\perp} - 2$), which corresponds to a significant exchange coupling [55]. Also, the value is typical of Cu(II) complex with tetragonal geometry.

The ratio $g_{||}/A_{||}$ is an empirical measure of the amount of tetrahedral distortion in copper complexes. Previous data gave a range of 105–135 cm^{-1} for square-planar geometry, and greater than 200 cm^{-1} for distorted tetrahedral geometry [56]. $[CuL.H_2O]_2$ gave $g_{||}/A_{||}$ value of 277 cm^{-1}, indicating its presence in a distorted tetrahedral geometry, which is in accord with the electronic spectra.

The σ-covalency parameter (α^2), which is a measure of covalency was calculated by the expression [57]

$$\alpha^2 = (A_{||}/0.036) + (g_{||} - 2.0023(+3/7(g \perp -2.0023) + 0.04,$$

(where $A_{||}$ is the copper nuclear hyperfine coupling constant expressed in cm^{-1} units) was found to be 0.566 for $[CuL.H_2O]_2$ complex.

The larger the α^2, the more covalent is the bond, from which it seems that this complex shows an extent of metal–ligand covalency.

3.1.5. Thermal analyses (TGA, DTG and DTA)

The thermogravimetric analyses of the studied complexes have been carried out and the thermodynamic parameters associated with the thermal reactions evaluated, Fig. 7. TGA and DTA of the ligands and their chelates were used to: (i) study the thermal stability of these complexes, (ii) decide whether the water molecules are coordinated to the central metal ions

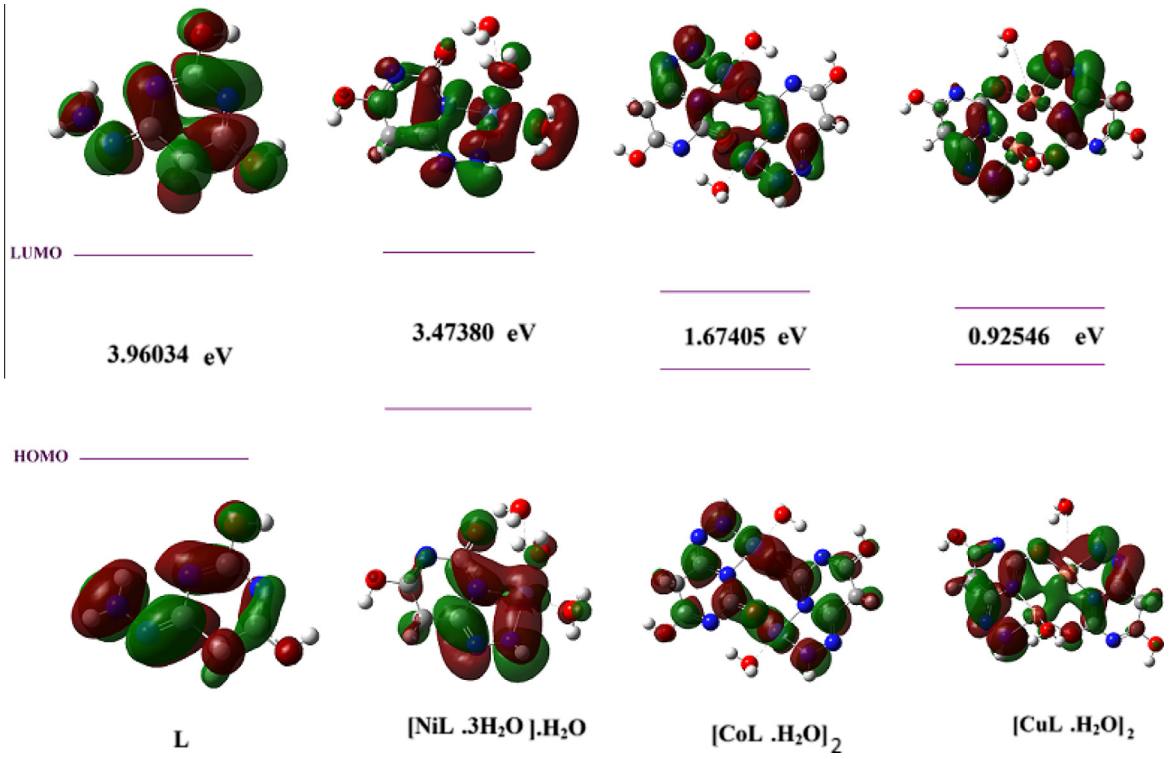

Figure 5 HOMO and LUMO energy levels of ligand and complexes.

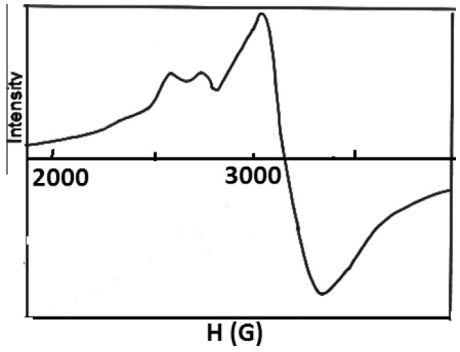

Figure 6 ESR spectrum of $[CuL.H_2O]_2$.

or present in ionic sphere -and (iii) suggest a general scheme for thermal decomposition of these chelates.(see Fig. 8).

The TGA of L showed that the ligand decomposed in a three decomposition step. The first starts between 0 and 228 °C with a mass loss (found: 19.05; calc.:19.58%) due to the loss of a CO molecule. The second step starts at 228–323 °C attributed to the loss of CO.CH molecule, (found: 28.57; calc.: 28.67%) and the third step between 323 and 471 °C due to the loss of N_2 + CH_2NHNH_2 molecules (found: 50.79; calc.: 51.05%) .

$[CoL.H_2O]_2$ was decomposed in multistep processes, where four steps were observed between (47–107, 107–213, 213–332 and 332–493 °C), respectively, as a result of eliminating ($2H_2O$ + $1/2N_2$), (steps one + two), with DTG_{max} = 62 and 150 °C, (found: 11.59; calc.: 11.53%), in step 3, $1/2N_2$ + N_2 + 2C were lost, (found: 15.21; calc.: 15.23%), with DTG = 314 °C and in step four, $2CH_2CONH$ + C molecules were lost (found: 29.59; calc.: 29.07%) with DTG = 374 °C and left with a residue of 43.22% corresponding to 2CoO + C (found: 42.69%) and formation of N_2 gas.

For $[NiL.3H_2O]H_2O$ complex, only two steps were obtained between (52–187 °C) and (187–631 °C) due to the loss of a H_2O molecule (found: 6.66; calc.: 6.62%) with DTG = 78 °C, then N_2 + $CH_2CH_2C(OH)NCN$ + 3 coordinated H_2O molecules (found: 66.66; calc.: 66.42%), DTG = 328, 375 and 448 °C and left with a residue of 26.67% attributed to NiO (calc.: 27.56%).

For $[CuL.H_2O]_2$, three steps between (26–140, 140–260 and 260–532 °C) were obtained as a result of the loss of $1/2N_2$ + H_2O molecules in the first step (found: 7.40; calc.: 7.22%), DTG = 41 & 110 °C, $1/2N_2$ + H_2O molecules in the second step (found: 7.80; calc.: 7.22%) DTG = 155 & 245 °C and $2CH_2CONH$ + C molecules in the third step (found: 27.98; calc.: 28.43%) DTG = (280, 325, 375, 440 and 507 °C) and left with a 56.82% due to the decomposition of the rest of the complex into $1.5N_2$ + 3C + 2CuO (56.66%).

Thermodynamic parameters associated with the thermal decomposition of the ligand and its complexes such as ΔE_a^* (activation energy), ΔH^* (enthalpy of reaction), n (order of reaction) and ΔS^* (entropy of reaction) were calculated using Horowitz–Metzger method [58], Table 3. Studies were not attempted for decomposition stages, which occur within a very narrow temperature range and data are not enough to be collected. The values of the decomposition reaction order (n) range between 0.8 and 2.0 showing a mixed regime of control (kinetic and diffusion). The negative values for the entropies of activation indicate that the activated complexes have more ordered structures than the reactants and that the reactions are slower than normal [59,60].

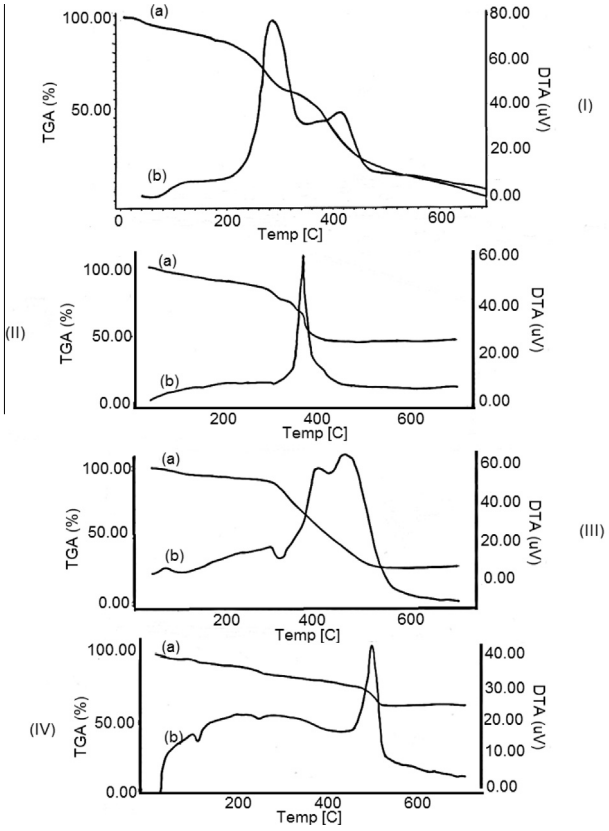

Figure 7 TGA and DTA curves of L and its complexes. (a): TGA, (b) DTA, (I) L (II) $[CoL.H_2O]_2$, (III) $[NiL.3H_2O].H_2O$, (IV) $[CuL.H_2O]_2$.

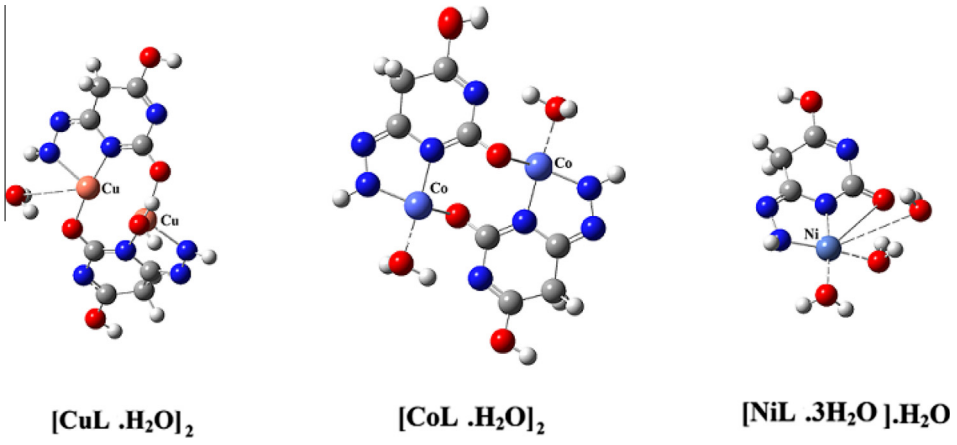

Figure 8 Structures of complexes.

Theoretically, the higher the value of the activation energy, the more stable is the complex which assigns the stability of the ligand L and its complexes. The activation energy of Co(II), Ni(II) and Cu(II) complexes was expected to increase in relation with decrease in their radius [61] as the smaller size of the ions permits a closer approach of the ligand. This was true for the last decomposition step for complexes where

- $\Delta E_{Cu} = 390.716$ kJ mole^{-1} > $\Delta E_{Ni} = 371.802$ kJ mole^{-1} > $\Delta E_{Co} = 272.616$ kJ mole^{-1}; r*Cu*(*II*) = 70 pm < r*Ni*(*II*) = 72 pm < rCo(*II*) = 74 pm.

From previous data, the structures of the ligand and complexes were deduced to be as follows:

3.2. Antibacterial and antifungal activities

Previous studies on the antibacterial activity of barbituric acid and its Co(II), Ni(II) and Cu(II) complexes against gram

Table 3 Thermodynamic parameters calculated from DTA data.

Compound	Peak	Shape	T_m	a	b	n	ΔE^* kJ mol^{-1}	α	Z	ΔH^* kJ mol^{-1}	ΔS^* kJ mol^{-1} K^{-1}
L	a	Exo	120	2.90	1.90	1.556	51.442	0.548	3.96	−27.108	−0.226
	b	Exo	294	3.00	3.70	1.134	136.116	0.608	3.36	−69.004	−0.234
	c	Exo	424	2.50	1.80	1.484	175.677	0.567	2.79	−101.460	−0.239
$[CoL.H_2O]_2$	a	Exo	375	2.3	1.90	1.386	272.616	0.570	5.52	−87.231	−0.232
$[NiL.3H_2O]H_2O$	a	Exo	75	0.65	0.90	1.070	64.433	0.619	34.15	−15.306	−0.204
	b	Endo	322	4.50	1.20	2.439	345.031	0.461	16.02	−71.641	−0.222
	c	Exo	459	6.00	2.30	2.035	371.802	0.496	10.03	−105.260	−0.229
$[CuL.H_2O]_2$.	a	Endo	113	0.50	0.40	1.408	225.393	0.567	167.08	−21.955	−0.194
	b	Endo	250	0.40	0.60	1.028	238.612	0.626	15.14	−55.214	−0.220
	c	Exo	499	1.00	2.15	0.859	390.716	0.659	9.46	−155.020	−0.230

Table 4 Antibacterial and antifungal activities of L and complexes.

Complex	Inhibition zone diameter (mm/mg sample)			
	Escherichia coli (G^-)	*Staphylococcus Aureus* (G^-)	*Aspergillus flavus* (Fungus)	*Candida albicans* (Fungus)
Tertacycline antibacterial agent	32	30	–	–
Amphotericin antifungal agent	–	–	19	20
Ligand	10	9		
$[CoL.H_2O]_2$	11	9	–	–
$[NiL.3H_2O]H_2O$	14	15	30	15
$[CuL.H_2O]_2$	10	11	–	–

positive (*S. aureus*) and gram negative bacteria (*E. coli*) revealed that neither barbituric acid nor its Cu(II) or Ni(II) complexes have any activity on these types of bacteria; however, the Co(II) complex has a good effect[62].

In this study, the synthesized compounds were screened for their antibacterial activity against *S. aureus* and *E. coli* and were evaluated in vitro for antifungal activity by using standard agar disk diffusion method [18,19] against *A. flavus* and *C. albicans*. The complexes under investigation showed considerable effect on both gram positive and gram negative bacteria much better than the complexes of barbituric acid and the most effect was seen by $[NiL.3H_2O]H_2O$. On the other hand, the study of the effect of these complexes on *A. flavus* and *C. albicans* fungi had also shown that the only effect was detected by $[NiL.3H_2O]H_2O$ complex, Table 4.

References

[1] M. Demeunynck, C. Bailly, W. David Wilson, Small molecule DNA and RNA binders: from synthesis to nucleic acid complexes, Wiley Online Library, (2004), doi: 10.1002/3527601783.

[2] (a) F. Hueso-Urena, N.A. Ilian-Cabeza, M.N. Moreno-Carretero, J.M. Martinez-Martos, M.J. Ramirez-Exposito, J. Inorg. Biochem. 94 (2003) 326–334;
(b) M.S. Refat, S.A. El-Korashy, A.S. Ahmed, Spectrochim. Acta 71A (2008) 1084–1094.

[3] A. Tsunoda, M. Shibisawa, Y. Yasuda, N. Nakao, K. Kusano, Anticancer Res. 14 (1994) 2637–2642.

[4] O. Sharma, B. Shrivastava, R.K. Singla, B.G. Varadaraj, Indo-Global J. Pharm. Sci. 1 (2011) 252–257.

[5] J.S. Casas, E.E. Castellans, M.D. Louce, J. Ellena, A. Sanchez, J. Sordo, C. Taboada, J. Inorg. Biochem. 11 (2006) 1858–1860.

[6] M.C. Rodriguez-Argüelles, M.B. Ferrari, G.G. Fava, C. Pelizzi, P. Tarasconi, R. Albertini, P.P. Dall'Aglio, P. Lunghi, S. Pinelli, J. Inorg. Biochem. 58 (1995) 157–175.

[7] J.S. Casas, M.S. Garcia-Tasende, C. Maichel-Mossmer, M.C. Rodriguez-Argüelles, A. Sanchez, J. Sordo, A. Vazquez-Lopez, S. Pinelli, P. Lunghi, R. Albertini, J. Inorg. Biochem 62 (1) (1996) 41–55.

[8] U. Koch, B. Attenni, S. Malancona, S. Colarusso, I. Conte, M.D. Filippo, S. Harper, B. Pacini, C. Giomini, S. Thomas, I. Incitti, L. Tomei, R.D. Francesco, S. Altamura, V.G. Matassa, F. Narjes, J. Med. Chem. 49 (5) (2006) 1693–1705.

[9] A. Ashnagar, N.G. Naseri, B. Sheeri, Chin. J. Chem. 25 (2007) 382–384.

[10] J.N. Delgado, J.N. Remers, Wilson and Gisvold's Textbook of Organic Medicinal Pharmaceutical Chemistry, nineth ed., L. Williams & Wilkins, Philadelphia, 1991, pp. 39, 341, 376..

[11] J.L. Fillaut, I. de los Rios, D. Masi, A. Romerosa, F. Zanobini, M. Peruzzini, Eur. J. Inorg. Chem. 2002 (4) (2002) 935–942.

[12] O.T. Arpaci, A. Ozdemir, I. Yalcin, I. Yildiz, E. Aki-Sener, N. Altanlar, Arch. Pharm. Chem. Life Sci. 338 (2–3) (2005) 105–111.

[13] N.M. Goudgaon, B.P. Sharanabasappa, G.J. Jyothi, J. Pharm. Res. 4 (7) (2011) 2195–2196.

[14] J. Fawcett, W. Henderson, R.D.W. Kemmitt, D.R. Russel, A. Upreti, J. Chem. Soc. Dalton Trans. 9 (1996) 1897–1903.

[15] L. Ma, S. Li, H. Zheng, J. Chen, L. Lin, X. Ye, Z. Chen, Q. Xu, T. Chen, J. Yang, N. Qiu, G. Wang, A. Peng, Y. Ding, Y. Wei, L. Chen, Eur. J. Med. Chem. 45 (2011) 2003–2010.

[16] (a) S. Rollas, S.G. Kucukguzel, Molecules 12 (2007) 1910–1939;
(b) F. Chimenti, E. Maccioni, D. Secci, A. Bolasco, P. Chimenti, A. Granese, O. Befani, P. Turini, S. Alcaro, F. Ortuso, M.C. Cardia, S. Distinto, J. Med. Chem. 50 (4) (2007) 707–712;
(c) E. Noulsri, R. Richardson, S. Lerdwana, S. Fucharoen, T. Yamagishi, D.S. Kalinowski, K. Pattanapanyasat, Am. J. Hematol. 84 (2009) 170–176.

[17] H.N. Bramson, J. Corona, S.T. Davis, S.H. Dickerson, M. Edelstein, S.V. Frye, R.T. Campe, P.A. Harris Jr., A. Hassell, W.D. Holmes, R.N. Hunter, K.E. Lackey, B. Lovejoy, M.J. Luzzio, V. Montana, W.J. Rocque, D. Rusnak, L. Shewchuk, J.M. Veal, D.H. Walker, L.F. Kuyper, J. Med. Chem. 44 (2001) 4339–4358.

[18] A.W. Bauer, W.M. Kirby, C. Sherris, M. Turck, Am. J. Clin. Pathol. 45 (1966) 493.
[19] M.A. Pfaller, L. Burmeister, M.A. Bartlett, M.G. Rinaldi, J. Clin. Microbiol. 26 (1988) 1437–1441.
[20] M.J. Frisch, G.W. Trucks, H.B. Schlegel, G.E. Scuseria, M.A. Robb, J.R. Cheeseman, G. Scalmani, V. Barone, B. Mennucci, G.A. Petersson, H. Nakatsuji, M. Caricato, X. Li, H.P. Hratchian, A.F. Izmaylov, J. Bloino, G. Zheng, J.L. Sonnenberg, M. Hada, M. Ehara, K. Toyota, R. Fukuda, J. Hasegawa, M. Ishida, T. Nakajima, Y. Honda, O. Kitao, H. Nakai, T. Vreven, J.A. Montgomery, Jr., J.E. Peralta, F. Ogliaro, M. Bearpark, J.J. Heyd, E. Brothers, K.N. Kudin, V.N. Staroverov, R. Kobayashi, J. Normand, K. Raghavachari, A. Rendell, J.C. Burant, S.S. Iyengar, J. Tomasi, M. Cossi, N. Rega, J.M. Millam, M. Klene, J.E. Knox, J.B. Cross, V. Bakken, C. Adamo, J. Jaramillo, R. Gomperts, R.E. Stratmann, O. Yazyev, A.J. Austin, R. Cammi, C. Pomelli, J.W. Ochterski, R.L. Martin, K. Morokuma, V.G. Zakrzewski, G.A. Voth, P. Salvador, J.J. Dannenberg, S. Dapprich, A.D. Daniels, Ö. Farkas, J.B. Foresman, J.V. Ortiz, J. Cioslowski, D.J. Fox, Gaussian Inc., Wallingford, CT, (2009).
[21] W. Kohn, L.J. Sham, Phys. Rev. 140 (1965) A1133–A1138.
[22] A.D. Becke, J. Chem. Phys. 98 (1993) 5648–5652.
[23] C. Lee, W. Yang, R.G. Parr, Phys. Rev. B37 (1998) 785–789.
[24] ÆFrisch, H.P. Hratchian, R.D. Dennington II, T.A. Keith, John Millam, B. Nielsen, A.J. Holder, J. Hiscocks. Gaussian, Inc., GaussView Version 5.0.8, (2009).
[25] M.H. Jamroz, Vibrational Energy Distribution Analysis, VEDA 4 Computer Program, Poland, (2004).
[26] N.P. Belskaya, W. Dehaen, V.A. Bakulev, ARKIVOC (i) (2010) 275–332.
[27] V.M. Vvedenskii, A.I. Zhvalevskaya, Chem. Heterocycl. Compd. 6 (1) (1970) 95–96.
[28] V. Berl, I. Huc, J.M. Lehn, A. DeCian, J. Fischer, Eur. J. Org. Chem. (1999) 3089–3094.
[29] B.G. Rao, U.C. Singh, J. Am. Chem. Soc. 113 (1991) 4381–4389.
[30] N. Hayashi, K. Sato, Y. Sato, M. Iwagami, N. Nishimura, J. Yoshino, H. Higuchi, T. Sato, J. Org. Chem. 76 (14) (2011) 5747–5758, http://dx.doi.org/10.1021/jo200852r.
[31] R.G. Lerner, B.P. Dailey, J.P. Friend, J. Chem. Phys. 26 (1957) 680–683, http://dx.doi.org/10.1063/1.1743367.
[32] I.L. Karle, J. Karle, J. Chem. Phys. 22 (1954) 43–45, http://dx.doi.org/10.1063/1.1739853.
[33] A. Saeed, I. Arshad, U. Flörke, J. Chem. (2013), Article ID 648121, http://dx.doi.org/10.1155/2013/648121.
[34] P. Labéguerie, M. Rohmer, M. Bénard, J. Chin. Chem. Soc. 56 (2009) 22–25.
[35] A.P. Scott, L. Random, J. Phys. Chem. 100 (1996) 16502–16513, http://dx.doi.org/10.1021/jp960976r.
[36] P. Pulay, G. Fogarasi, G. Pongor, J.E. Boggs, A. Vargha, J. Am. Chem. Soc. 105 (24) (1983) 7037–7047.
[37] J.A. Pople, H.B. Schlegel, R. Krishnan, D.J. Defrees, J.S. Binkley, M.J. Frisch, R.A. Whiteside, R.F. Hout, W.J. Hehre, Int. J. Quantum Chem. Symp. 15 (1981) 269–278.
[38] D.A. Chowdhury, M.N. Uddin, A.H. Sarker Md, Chiang Mai J. Sci. 35 (3) (2008) 483–494.
[39] S. Gunasekaran, S.R. Varadhan, K. Manoharan, Asian J. Phys. 2 (1993) 165–172.
[40] D. Sajan, J. Binoy, B. Pradeep, K. Venkatakrishnan, V.B. Kartha, I.H. Joe, V.S. Jayakumar, Spectrochim. Acta Part 60A (2004) 173–180.
[41] N. Sundaraganesan, S. Ilakiamani, P. Subramanian, B.D. Joshua, Spectrochim. Acta 67A (2007) 628–635.
[42] P. Tharmaraji, D. Kodimunthiri, C.D. Sheela, C.S.S. Priya, J. Serb. Chem. Soc. 74 (2009) 927–938.
[43] J. Pople, W.G. Schneider, H.J. Bernstein, High-Resolution Nuclear Magnetic Resonance, Wiley, New York, Toronto, London, 1959.
[44] J.C. Davis, K.S. Pitzer, J. Phys. Chem. 64 (1960) 886–892.
[45] H.G. Beaton, G.R. Willey, M.G.B. Drew, J. Chem. Soc. Perkin Trans. 2 (1987) 469–472.
[46] G. Zuchowski, K. Zborowski, Cent. Eur. J. Chem. 4 (3) (2006) 523–532.
[47] R.M. Aminova, G.A. Schamov, A.V. Aganov, J. Mol. Struct. (Theochem.) 498 (2000) 233–246.
[48] M. Kidwai, R. Thakur, R. Mohan, Acta Chim. Slov. 52 (2005) 88–92.
[49] M. Hamming, N. Foster, Interpretation of Mass Spectra of Organic Compounds, Academic Press, New York, USA, 1972.
[50] I. Fleming, Frontier Orbitals and Organic Chemical Reactions, John Wiley and Sons, New York, 1976.
[51] G.G. Mohamed, M.M. Omar, A.M. Hindy, Turk. J. Chem. 30 (2006) 361–382.
[52] G. Kumar, D. Kumar, S. Devi, R. Verma, R. Johari, Int. J. Eng. Sci. Technol. 3 (2) (2011) 1630–1635.
[53] B.H.M. Mruthunjayaswamy, O.B. Ijare, Y. Jadegoud, J. Braz. Chem. Soc. 16 (2005) 783–789.
[54] M.S. Masoud, A.A. Soayed, A.E. Ali, O.K. Sharsherh, J. Coord. Chem. 56 (2003) 725–742.
[55] B.J. Hathaway, D.E. Billing, Coord. Chem. Rev. 5 (1970) 143–207.
[56] M.S. Masoud, E.A. Khalil, A.M. Hafez, A.F. El-Husseiny, Spectrochim. Acta A 61 (2005) 989–993.
[57] D. Kivelson, R. Neiman, J. Chem. Phys. 35 (1961) 149–155.
[58] H.H. Horowitz, G. Metzger, Anal. Chem. 35 (1963) 1464–1468.
[59] M. Padmanabhan, S.M. Kumary, X. Huang, J. Li, Inorg. Chim. Acta 358 (2005) 3537–3544.
[60] A.A. Frost, R.G. Pearson, Kinetics and Mechanism, Wiley, NewYork, 1961.
[61] G. Avsar, N. Kulcu, H. Arslan, Turk. J. Chem. 26 (2002) 607–615.
[62] A.A. Ikotun, Y. Ojo, C.A. Obafemi, G.O. Egharevba, Afr. J. Pure Appl. Chem. 5 (5) (2011) 97–103.